*J. Zool., Lond.* (2004) **264**, 327–332 © 2004 The Zoological Society of London Printed in the United Kingdom DOI:10.1017/S0952836904005813

# Aerodynamic forces of revolving hummingbird wings and wing models

Douglas L. Altshuler[1]*, Robert Dudley[1,2,3] and Charles P. Ellington[4]

[1] Section of Integrative Biology, University of Texas at Austin, Austin, Texas, 78712, U.S.A.
[2] Smithsonian Tropical Research Institute, P.O. Box 2072, Balboa, Republic of Panama
[3] Present Address: Department of Integrative Biology, University of California, Berkeley, CA 94720, U.S.A.
[4] Department of Zoology, University of Cambridge, Cambridge CB2 3EJ, U.K.

*(Accepted 1 April 2004)*

**Abstract**

A central challenge to the study of animal aerodynamics has been the measurement of forces generated by flapping wings. Relative to wings of other birds, hummingbird wings are of particular interest in that the smaller species operate in more viscous regimes ($5000 < Re < 10\,000$) for which substantial drag and reduced lift:drag coefficients might be expected. Lift and drag forces were measured on mounted hummingbird wings and wing models spinning in continuous tipwise revolution about the wing base. Lift coefficients tended to increase as wing models became more realistic (i.e. with sharpened leading edges and with substantial camber). Lift:drag ratios of real wings were substantially higher than those of wing models, suggesting morphological contributions of feathers to lift enhancement and drag reduction. At $Re = 5000$, high values of the lift:drag ratio (8–16) at low angles of attack suggest that wings of hummingbirds are exceptionally good at producing lift.

**Key words**: aerodynamics, angle of attack, camber, hummingbird, leading edge, model wings

## INTRODUCTION

The flight of insects, encompassing broadly a Reynolds number (*Re*) range of 10–10 000, represents an important area of investigation into unsteady aerodynamic mechanisms. In particular, the use of models of dynamically scaled flapping wings has revealed unsteady lift coefficients substantially higher than those previously recognized (Ellington *et al.*, 1996; Dickinson, Lehmann & Sane, 1999). For larger insects such as hawkmoths, pronounced leading-edge separation and a spiral leading-edge vortex (LEV) yield sufficient lift and associated vertical forces necessary for flight (van den Berg & Ellington, 1997*a*,*b*). Similar lift enhancement occurs at the lower *Re* characteristic of fruitflies (Dickinson *et al.*, 1999; Sane & Dickinson, 2001, 2002), although the spiral nature of the LEV in this context is less pronounced (see Birch & Dickinson, 2001).

Hummingbirds represent an important taxon with which to evaluate the importance of such unsteady aerodynamic mechanisms in that the interspecific hovering range of *Re* for the wings (~ 5000–30 000) probably spans a transition from laminar to turbulent flow. Minute structural details of avian wings may also alter their aerodynamic properties. For example, the rachis of the 10th primary feather in hummingbirds extends parallel to the wing's leading edge for the distal portion of the wing length, protruding 0.2–0.3 mm above the feather's surface much like turbulator strips (pers. data) – structures that reduce drag by initiating turbulent boundary layers. In hovering flight, the mean lift coefficients required for weight support by hummingbirds are comparable to those for insects (Weis-Fogh, 1972, 1973; Ellington, 1984*a*), so that substantial force enhancement relative to lift production under steady flow may be expected.

Accurate replication of animal flapping motions is difficult, but for a diversity of insect wing planforms and for an actual quail wing, high lift production is a robust characteristic of continuously revolving wings (Usherwood & Ellington, 2002*a*,*b*). By continuously rotating wings as propeller blades at a constant angular velocity about a vertical axis, time-averaged vertical and horizontal forces can be measured using either force transducers mounted at the wing base or by placing the entire apparatus on balances. Adjusting either wing orientation or angular velocity allows for distinct lift and drag measurements to be made over a range of angles of attack ($\alpha$) and *Re*, respectively. This approach using wings in continuous revolution will reveal aerodynamic forces produced during continuous translation with strong spanwise flow, but necessarily excludes those forces associated with pronation and supination. Although biologically less realistic,

*All correspondence to present address: D. L. Altshuler, California Institute of Technology, Mail Code 138-78, 1200 East California Boulevard, Pasadena, CA 91125, U.S.A. E-mail: doug@caltech.edu

continuously revolving wings may nonetheless reveal novel features of design that enhance unsteady lift production. In the present work, a suite of hummingbird wing models was constructed based on actual planforms that varied in thickness, sharpness of the leading edge, and camber. Comparisons in aerodynamic force coefficients were made among these models, and also between the models and the actual wing of a hummingbird.

## METHODS

### Model wings

Wing models were tested on a medium-sized propeller rig. A complete description and schematic of the apparatus are presented elsewhere (Ellington & Usherwood, 2001) and only a brief description will be given here. Wing models were mounted to a rotor head allowing fine adjustment of the angle of attack. The rotor head was attached to a motor (12 V DC/15 W) mounted in two ball-races at the base of the rig; the motor was free to rotate in response to the motor reaction torque. This torque was measured via a mechanical arm connected to the motor case and abutting a beam that pivoted on a razor blade. The far end of the beam inserted at a point contact downwards on the measuring surface of a balance (Mettler PG2002-S), effectively converting the horizontal force into a vertical one. Torque balance readings were calibrated by hanging a known weight from the torque arm. Measurement of vertical forces was accomplished by attaching the base of the rig to a second digital balance. Both balances were shielded from propeller downwash by a large piece of cardboard. Balance readings were averaged over 20 s, and 3 readings were made for each combination of $\alpha$ and *Re*.

Balance readings (g) were converted into non-dimensional vertical $C_v$ and horizontal $C_h$ force coefficients using a blade element analysis following Ellington & Usherwood (2001). These force coefficients were then used to calculate lift ($C_L$) and drag ($C_D$) coefficients that incorporated the downwash angle (see Usherwood & Ellington, 2002*a*).

The planform of the wing models was based on an image of the left wing of a female ruby-throated hummingbird *Archilochus colubris* with a wing length of 46.5 mm and an aspect ratio of 7.72. In contrast to the wing, the models did not possess scalloped trailing edges derived from feathers, and instead had a smooth trailing edge. The model wing was considerably larger (length 100 mm, aspect ratio 7.65) but was designed to closely match the planform of the wing using the non-dimensional radii of the moments of wing area (Ellington, 1984*b*). The respective values for the first, second, and third radii were 0.422, 0.494, and 0.546 for the real wing, and 0.422, 0.494, and 0.547 for the models. The models were constructed in pairs and were measured as such on the rig to eliminate inertial imbalance during spinning.

Two sets of experiments were performed using model wings. In the first set, both horizontal and vertical forces were measured across a range of angles of attack ($-5°$ to $50°$ at $5°$ intervals) and of angular velocities (corresponding to a *Re* of 5000 and 10 000). Three pairs of model wings were tested. The first pair was made of flat perspex with a thickness of 2 mm, corresponding to 7.75% of the mean chord. The leading edge was sanded at 45°, such that the perimeter of the dorsal wing planform was 2 mm wider than the ventral planform. Thus, at high $\alpha$ (e.g. $> 45°$), the leading edge was effectively perpendicular with respect to the oncoming airflow. This model is hereafter referred to as 'bevelled perspex'. The second pair of models was thinner (thickness of 0.4 mm, corresponding to 1.55% of the mean chord), and was made of aluminium with a highly sharpened edge. Both dorsal and ventral sides of the leading edge were sanded at a sharp angle (*c.* 60°) so that the leading edge was sharp at all angles of attack. These models are hereafter referred to as 'sharpened aluminium'. The third pair of wing models was cut from a brass pipe to produce models with camber. These models were 1 mm thick (representing 3.68% of the mean chord), had a symmetrically sharpened leading edge at *c.* 60°, and a camber value of 5%. Angle of attack was measured for the wing chord located two-thirds of the distance from the axis of rotation to the wing tip. These wings are hereafter referred to as 'cambered brass'.

In a second set of model wing experiments, the lift forces were measured on model wings that differed in 2 morphological properties: thickness and shape of the leading edge. Three thickness values were considered (0.4, 0.9 and 1.5 mm; corresponding to 1.55%, 3.49%, and 5.81% of the mean chord, respectively), as were 2 leading edge morphologies: straight and bevelled. Straight leading edges were cut perpendicular to the plane of the wing. At high angles of attack ($> 45°$), the straight models had sharp leading edges relative to oncoming flow. Bevelled wings had a leading edge similar to the bevelled wings used in the first experiment (sharpened at 45°) and thus presented blunt leading edges at high angles of attack. Accordingly, 6 pairs of possible morphological combinations were tested on the propeller rig. The 3 pairs of models with sharp leadings edges were first measured, and were then sanded at the leading edge to produce a bevelled edge. The 6 total pairs of wing models were measured at $\alpha = 45°$ and at 2 rotational speeds corresponding to *Re* of 5000 and 10 000.

### Real hummingbird wing

An actual wing from a female rufous hummingbird *Selasphorus rufus* (*Re* ~ 7000 during hovering) was tested on a smaller propeller rig (the mini-spinner) as the real wing was considerably smaller than the wing models first tested. A complete description and schematic of the mini-spinner are presented elsewhere (Usherwood & Ellington, 2002*b*). The real wing was first mounted onto a small (1 mm diameter) metal tube (Fig. 1). This tube was then inserted into a slot in the propeller head; the rotational angle of the mounting tube and thus $\alpha$ of the wing could be set using a protractor, with the mounting tube then secured via a grub

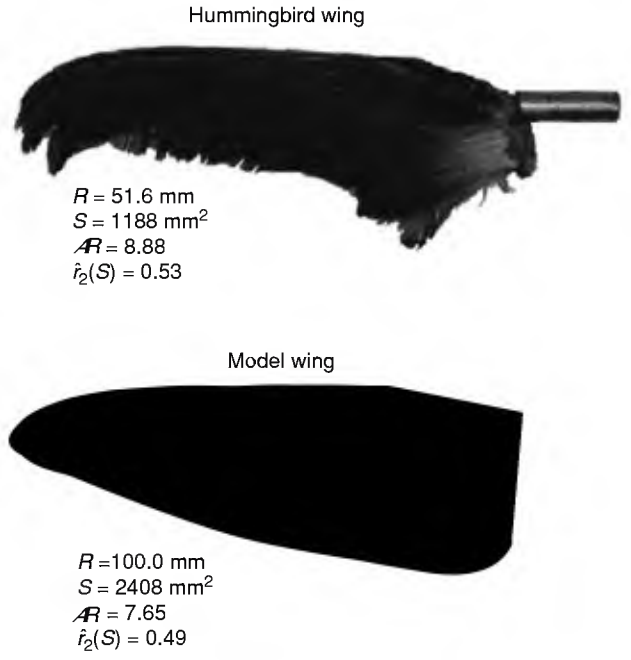


**Fig. 1.** Planform images of real hummingbird wing of the *Selasphorus rufus* female and model wings used in experiments. Morphological values: $R$, wing length; $S$, wing area; $AR$, aspect ratio; $\hat{r}_2(S)$, non-dimensional radius of second moment of wing area. The original hummingbird wing was modified by removing the feathers near the base of the wing to facilitate mounting on mini-spinner.

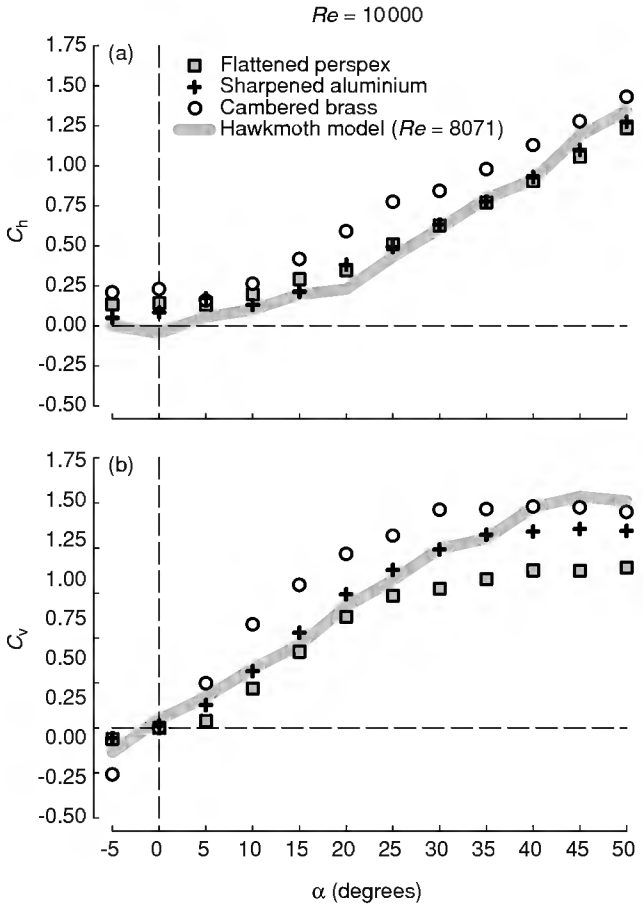


**Fig. 2.** Non-transformed force coefficients for model wings at $Re = 10\,000$. Coefficients of horizontal $C_h$ (a) and vertical $C_v$ (b) force are plotted as a function of angle of attack $\alpha$. Results from a hawkmoth model wing ($Re$ = 8071) under 'steady' conditions of Usherwood & Ellington (2002*a*) are included for comparison.

screw. The angle of attack was measured for the wing chord at two-thirds of the wing length for the stationary wing. Only 1 wing was attached because an identical wing (as opposed to the contralateral wing from the same individual) was obviously unavailable. The propeller head was attached to a motor located at the end of a moment arm fitted with a razor-blade fulcrum. Moments generated by the propeller head were thus transferred with equal and opposite force to the opposite end of the moment arm. The far end of the moment arm was attached with a fine wire to the underhook of a balance (Mettler BaBal BB240). Vertical forces and torques were measured separately. For the former, the motor, gearbox and propeller head were all oriented vertically. Conversely, aerodynamic torques were measured by reorienting the motor, gearbox and propeller head to a horizontal position. Measurements on the balance were averaged over 9 s; 3 readings were taken for each value of $\alpha$ and $Re$. Force coefficients were estimated using the same equations as for the model wings and were compared with model wings from experiment 1.

## RESULTS

### Experiment 1

Horizontal force coefficients for model wings spinning at a $Re$ of 10 000 are given in Fig. 2a. The cambered model had the highest horizontal force coefficient at all values of $\alpha$ except at 5°, for which value the horizontal force was equal to that of the other two models. The two flat models had equal horizontal forces for $\alpha > 15°$. Thus, sharpness of the leading edge did not influence horizontal force at high angles of attack. Model wings varied even more substantially in vertical forces (Fig. 2b). The cambered brass model exhibited the highest vertical force, followed by the sharpened aluminium, and lastly by the bevelled perspex. This pattern held for all positive angles of attack.

The real wing measured on the mini-spinner became unstable at high speeds owing to uneven force transfer from the moment arm to the balance. Only values at $Re = 5000$ are accordingly presented (Fig. 3). The results for both the real wing and the models were more variable than for measurements at the higher $Re$ (cf. Fig. 2). The real wing incurred substantially less horizontal force during continuous revolution, particularly at $\alpha > 25°$, and produced substantially more vertical force for $\alpha > 5°$.

For comparison among the models and with published data, transformed force coefficients are plotted in a polar diagram in Fig. 4a. The bevelled perspex model yielded the least lift. The sharpened aluminium model generated

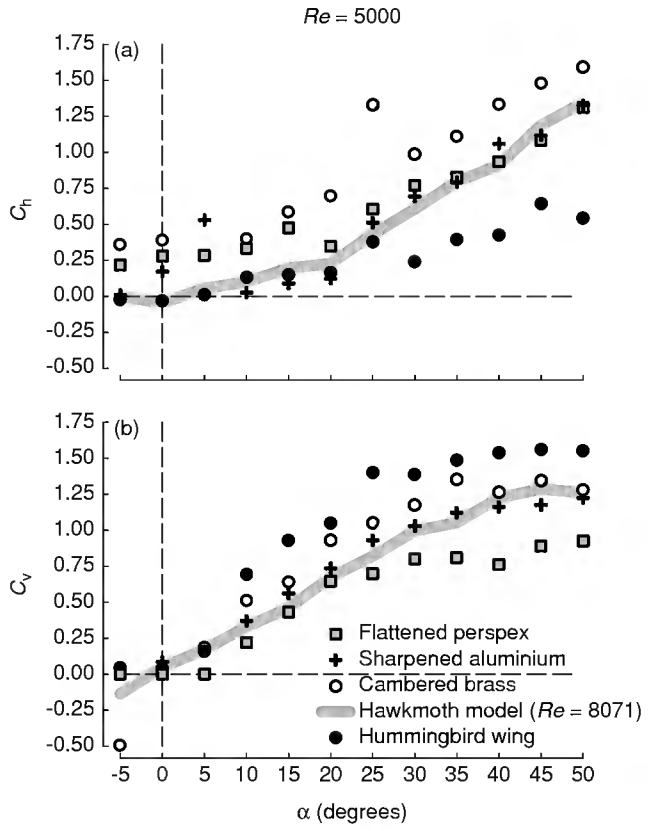


**Fig. 3.** Non-transformed force coefficients for model wings and for a hummingbird wing at $Re = 5000$. Other figure characteristics as in Fig. 2.

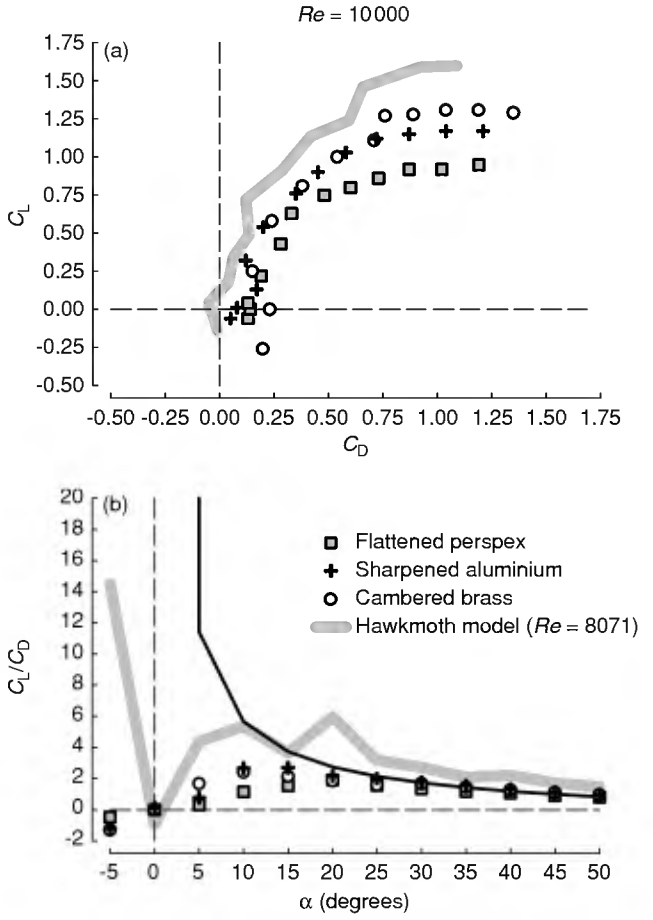


**Fig. 4.** Differences in performance among model wings at $Re = 10\,000$. Transformed coefficients of lift $C_L$ and drag $C_D$ were calculated using the large angle, 'swirl' algorithm of Usherwood & Ellington (2002*a*). (a) Polar diagram comparing $C_L$ and $C_D$; (b) lift-to-drag ratio together with cot $\alpha$ plotted as a function of $\alpha$ (solid black line).

substantially greater lift with only slightly greater drag. The cambered brass model produced both greater lift and drag at all positive angles of attack. Conversely, the cambered hawkmoth model studied by Usherwood & Ellington (2002*a*), which bears the strongest resemblance in terms of relative thickness to an actual insect wing (thickness was less than 1.6% of the mean chord), also exhibited the best performance in terms of high lift and low drag (see Fig. 4a).

Knowledge of the lift:drag ratio allows for a simple test of the presence of a specific aerodynamic mechanism, namely a leading-edge vortex (LEV; see Ellington & Usherwood, 2001). In delta-wing aircraft, a LEV creates a large suction force normal to the wing such that the induced drag owing to lift divided by the total lift is simply equal to the tangent of $\alpha$ (Polhamus, 1971). The lift-to-drag ratios of our wing models at $Re = 10\,000$ are plotted as a function of $\alpha$ and compared to cot $\alpha$ in Fig. 4b. The fit between the models and cot $\alpha$ is good at high $\alpha$, suggesting that suction produced by a LEV underlies force production.

The polar diagram for the models and the real hummingbird wing at $Re = 5000$ reveals more curious patterns (Fig. 5). The lift/drag curve for the real wing is markedly steeper than that for all of the models, indicating much higher performance with lower drag and greater lift (Fig. 5a). The lift:drag ratio of the real wing at high angles of attack is considerably greater than the theoretical prediction of the cot $\alpha$ curve associated with a LEV (Fig. 5b), indicating that leading-edge vorticity may not account for the majority of force on the real wing.

## Experiment 2

Vertical force coefficients of models wings used in experiment 2 are given in Table 1. Coefficients were similar at $Re$ of 5000 and 10 000. Models with a moderately sharp leading edge (straight) generated substantially larger vertical force coefficients than did models with bevelled edges at this high angle of attack. The effects of wing thickness were less clear. Considering first the bevelled wings, vertical force decreased with increasing thickness. For the non-bevelled models, the vertical forces seem to be independent of thickness. One anomaly is the value for the non-bevelled 0.9 mm thick model at $Re = 5000$, which is substantially smaller than the value for those models at $Re = 10\,000$. This unusually small value for the vertical

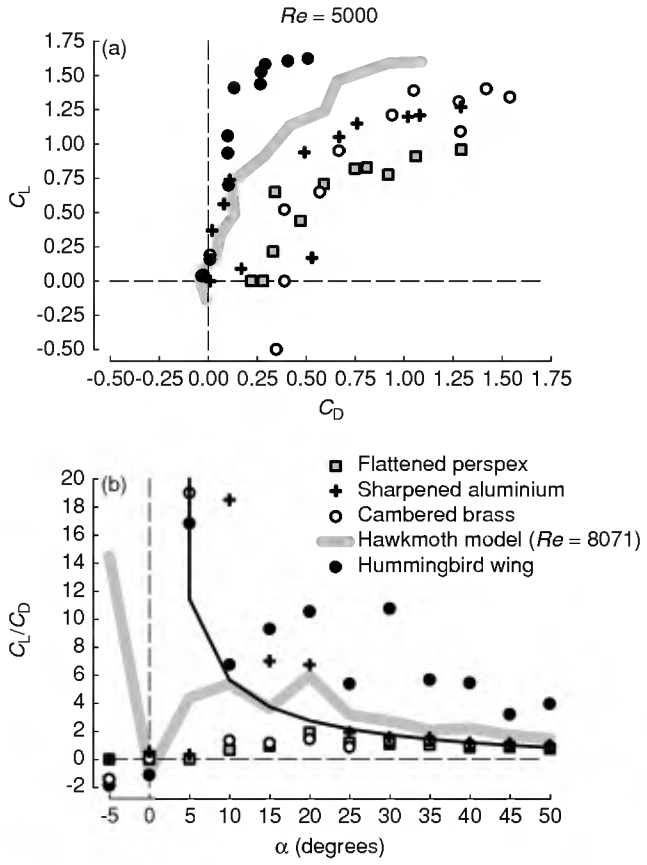


**Fig. 5.** Differences in performance among real and model hummingbird wings at $Re = 5000$. Other figure characteristics as in Fig. 4.

**Table 1.** Vertical force coefficients for model wings at $\alpha = 45°$. Values are means with standard deviations in parentheses ($n = 3$). Models were constructed of flat aluminium of varying thickness. Wings were first tested with a sharp edge (cut perpendicular to wing chord), and were then bevelled by sanding the leading edge dorsally at 45°

| | | Reynolds no. | |
|---|---|---|---|
| Thickness (mm) | Leading edge | 5000 | 10 000 |
| 0.4 | Sharp | 1.08 (0.02) | 1.06 (0.02) |
| 0.4 | Bevelled | 0.98 (0.06) | 1.02 (0.01) |
| 0.9 | Sharp | 1.01 (0.02) | 1.06 (0.01) |
| 0.9 | Bevelled | 0.98 (0.02) | 0.96 (0.01) |
| 1.55 | Sharp | 1.09 (0.01) | 1.09 (0.01) |
| 1.55 | Bevelled | 0.93 (0.00) | 0.92 (0.01) |

force coefficient deviates from the above patterns, and may have resulted from experimental error.

## DISCUSSION

Overall, these aerodynamic data for revolving wings demonstrate important consequences of wing morphology and leading-edge geometry for unsteady force production. Model wings of equivalent planform and operated at identical *Re* differed substantially according to absolute thickness and the extent of sharpness (Table 1). Lift decline following ventral bevelling of the leading edge was particularly pronounced; such a geometrical asymmetry presents a relatively greater surface to oncoming flow when the wing is oriented at intermediate to high angles of attack, rendering the edge more thick and reducing vertical force and associated lift production. By contrast, sharpening of both dorsal and ventral surfaces of the leading edge for wing models (i.e. symmetric edge sharpening) enhanced vertical forces and lift production relative to asymmetrically bevelled models (Figs 2–4). Symmetric sharpening of the leading edge combined with camber tended, not surprisingly, to enhance further the vertical force and lift coefficients, albeit with the cost of greater drag. The sensitivity of force production to leading-edge details and wing thickness suggest that small-scale geometrical features contributing to vortex initiation and growth at or near the leading edge are important contributors to the overall flow pattern on the wing, a point not generally recognized in the animal flight literature. The LEV on wing models, the presence of which is suggested by the relationship between lift:drag ratios and the cotangent of the angle of attack (Fig. 4b), is an obvious candidate for such aerodynamic interactions.

Enhanced lift performance of a real hummingbird wing relative to equivalent planform models suggests further aerodynamic relevance of wing structural details. Deformability and partial permeability of feathers together with milliscale morphological projections from feather rachides could all potentially influence unsteady flow near the leading edge. Unlike hummingbird wing models and a model hawkmoth wing at comparable *Re* (~ 8000; Usherwood & Ellington, 2002*a*), the real hummingbird wing used here deviated substantially from aerodynamic performance predicted for a LEV alone. High lift and reduced drag (Fig. 5) sharply distinguish the actual wing from wing models. The unsteady aerodynamics of hummingbirds may thus be qualitatively different from that of large hovering insects such as *Manduca sexta* for which body weight support effected via a LEV is sufficient (van den Berg & Ellington, 1997*a*,*b*). Flow visualization and velocimetry measurements on revolving hummingbird wings would evaluate this possibility.

Although the angle of attack can be easily measured for flat plates, this metric must be defined more precisely for airfoils with camber or other three-dimensional structure. For our cambered wing model, $\alpha$ was defined using the angle of the wing chord at two-thirds wing length, and not with the zero-lift angle. The real hummingbird wing is more deformable than our wing models, and $\alpha$ likely changes with wingtip velocity as well as along the wing length. The influence of deformation in animal wings on aerodynamic force production is not well understood, and would provide a highly informative avenue for future investigation.

Hummingbirds in flight evidence further kinematic features that may augment unsteady force production. Relatively high wingbeat frequencies and considerable

wing rotation at the ends of half-strokes (to date not quantified, but probably exceeding 90°) indicate high angular velocities and associated rotational contributions to lift production (Ellington, 1984*c*; Sane & Dickinson, 2002). Interspecifically, hovering hummingbirds also exhibit allometries of wing area and wingbeat frequency significantly more positive and more negative, respectively, than those of insects (Dudley, 2002; Altshuler & Dudley, 2003). Mean lift coefficients in hovering vary inversely with the square of wingbeat frequency, so that larger hummingbird species will experience exacerbated lift requirements. Relative increases in wing area will partially offset such demand, but the possibility of specialized lift-enhancing features such as rachis turbulators is an exciting question for future allometric studies.

**Acknowledgements**

We dedicate this paper to Robin Wootton in recognition of his long and distinguished career studying animal flight. We thank James R. Usherwood for valuable discussions during the course of the study and Michael H. Dickinson and William Dickson for critique of the manuscript. Funding for this research was provided by grants from the National Science Foundation (IBN 9817138 and IBN 992155).

## REFERENCES

Altshuler, D. L. & Dudley, R. (2003). Kinematics of hovering hummingbird flight along simulated and natural elevational gradients. *J. exp. Biol.* **206**: 3139–3147.

Birch, J. M. & Dickinson, M. H. (2001). Spanwise flow and the attachment of the leading-edge vortex on insect wings. *Nature (Lond.)* **412**: 729–733.

Dickinson, M. H., Lehmann, F.-O. & Sane, S. P. (1999). Wing rotation and the aerodynamic basis of insect flight. *Science* **284**: 1954–1960.

Dudley, R. (2002). Mechanisms and implications of animal flight maneuverability. *Integr. comp. Biol.* **42**: 135–140.

Ellington, C. P. (1984*a*). The aerodynamics of hovering insect flight. I. The quasi-steady analysis. *Philos. Trans. R. Soc. Lond. B Biol. Sci.* **305**: 1–15.

Ellington, C. P. (1984*b*). The aerodynamics of hovering insect flight. II. Morphological parameters. *Philos. Trans. R. Soc. Lond. B Biol. Sci.* **305**: 17–40.

Ellington, C. P. (1984*c*). The aerodynamics of hovering insect flight. IV. Aerodynamic mechanisms. *Philos. Trans. R. Soc. Lond. B Biol. Sci.* **305**: 79–113.

Ellington, C. P. & Usherwood, J. R. (2001). Lift and drag characteristics of rotary and flapping wings. In *Fixed and flapping wing aerodynamics for micro air vehicle applications* **195**: 231–248. Mueller, T. J. (Ed.). Reston, VA: American Institute of Aeronautics and Astronautics.

Ellington, C. P., van den Berg, C., Willmott, A. P. & Thomas, A. L. R. (1996). Leading-edge vortices in insect flight. *Nature (Lond.)* **384**: 626–630.

Polhamus, E. C. (1971). Predictions of vortex–lift characteristics by a leading-edge suction analogy. *J. Aircraft* **8**: 193–199.

Sane, S. P. & Dickinson, M. H. (2001). The control of flight force by a flapping wing: lift and drag production. *J. exp. Biol.* **204**: 2607–2626.

Sane, S. P. & Dickinson, M. H. (2002). The aerodynamic effects of wing rotation and a revised quasi-steady model of flapping flight. *J. exp. Biol.* **205**: 1087–1096.

Usherwood, J. R. & Ellington, C. P. (2002*a*). The aerodynamics of revolving wings I. Model hawkmoth wings. *J. exp. Biol.* **205**: 1547–1564.

Usherwood, J. R. & Ellington, C. P. (2002*b*). The aerodynamics of revolving wings II. Propeller force coefficients from mayfly to quail. *J. exp. Biol.* **205**: 1565–1576.

van den Berg, C. & Ellington, C. P. (1997*a*). The vortex wake of a 'hovering' model hawkmoth. *Philos. Trans. R. Soc. Lond. B Biol. Sci.* **352**: 317–328.

van den Berg, C. & Ellington, C. P. (1997*b*). The three-dimensional leading-edge vortex of a 'hovering' model hawkmoth. *Philos. Trans. R. Soc. Lond. B Biol. Sci.* **352**: 329–340.

Weis-Fogh, T. (1972). Energetics of hovering flight in hummingbirds and in *Drosophila*. *J. exp. Biol.* **56**: 79–104.

Weis-Fogh, T. (1973). Quick estimates of flight fitness in hovering animals, including novel mechanisms for lift production. *J. exp. Biol.* **59**: 169–230.